SUPPLEMENTARY DATA

Truncated stathmin-2 is a marker of TDP-43 pathology in frontotemporal dementia

Authors: Mercedes Prudencio, Jack Humphrey, Sarah Pickles, Anna-Leigh Brown, Sarah E. Hill, Jennifer M. Kachergus, J. Shi, Michael G. Heckman, Matthew R. Spiegel, Casey Cook, Yuping Song, Mei Yue, Lillian M. Daughrity, Yari Carlomagno, Karen Jansen-West, Cristhoper Fernandez de Castro, Michael DeTure, Shunsuke Koga, Ying-Chih Wang, Prasanth Sivakumar, Cristian Bodo, Ana Candalija, Kevin Talbot, Bhuvaneish T. Selvaraj, Karen Burr, Siddharthan Chandran, Jia Newcombe, Tammaryn Lashley, Isabel Hubbard, Demetra Catalano, Duyang Kim, Nadia Propp, Samantha Fennessey, NYGC ALS Consortium, Delphine Fagegaltier, Hemali Phatnani, Maria Secrier, Elizabeth M. C. Fisher, Björn Oskarsson, Marka van Blitterswijk, Rosa Rademakers, Neil R. Graff-Radford, Bradley F. Boeve, David S. Knopman, Ronald C. Petersen, Keith A. Josephs, E. Aubrey Thompson, Towfique Raj, Michael Ward, Dennis W. Dickson, Tania F. Gendron, Pietro Fratta, Leonard Petrucelli.

Corresponding authors: Leonard Petrucelli, Department of Research, Neuroscience, Mayo Clinic College of Medicine, 4500 San Pablo Rd, Jacksonville, FL 32224. 1-904-953-2855, petrucelli.leonard@mayo.edu; and Pietro Fratta, Department of Neuromuscular Diseases, UCL Queen Square Institute of Neurology, Queen Square, London, WC1N 3BG, +44(0)2034484112, p.fratta@ucl.ac.uk.

Supplementary Methods

Human iPSC culture and neuronal differentiation

CRISPRi-i^{3}Neuron iPSCs were generated from a control iPSC line (WTC11) that harbors a dox-inducible mouse NGN2 transgene at the AAVS1 locus (i3N) (1), and that stably expresses dCas9-BFP-KRAB via TALEN-mediated integration of CAG-dCas9-BFP-KRAB into the CLYBL safe harbor locus (2). Human iPSCs were maintained as previously described (1, 3). In brief, iPSCs were cultured in Essential 8 Medium (Thermo Fisher Scientific) in cell culture dishes pre-coated with Phenol-free Matrigel Basement Membrane Metrix (Corning) diluted 1 in 100 in Knock-out DMEM (Thermo Fisher Scientific). For passaging, media was aspirated, cells were washed in Dulcecco's phosphate buffered saline (DPBS, Thermo Fisher Scientific), incubated in StemPro Accutase (Thermo Fisher Scientific) and diluted in DPBS. The cell suspension was centrifuged at 200 x g for 5 minutes and resuspended in Essential 8 Medium supplemented with 10 nM Thiazovivin (Millipore). For differentiation into iPSC-derived neurons, cells were pelleted and then resuspended in N2 Pre-Differentiation Medium [Knock-out DMEM/F12 (Thermo Fisher Scientific) supplemented with 1X MEM Non-Essential Amino Acids (Thermo Fisher Scientific), 1X N2 Supplement (Thermo Fisher Scientific), 10 nM Thiazovivin and 2 µg/mL doxycycline hydrochloride (Sigma-Aldrich)] and plated at the desired number on Matrigel-coated plates for 72 hours. Pre-differentiated cells were passaged as described above and the pelleted cells were resuspended in Neuronal Medium [half DMEM/F12 (Thermo Fisher Scientific), half Neurobasal A (Thermo Fisher Scientific) supplemented with 1X MEM Non-Essential Amino Acids. 0.5X GlutaMAX supplement (Thermo Fisher Scientific), 0.5X N2 Supplement, 0.5X B27 Supplement (Thermo Fisher Scientific), 10 ng/mL NT-3 (Pepro-Tech), 10 ng/mL BDNF (Pepro-Tech), 1 µg/mL Mouse Laminin (Invitrogen]) and plated on cell culture dished pre-coated with poly-L-ornathine (Sigma-Aldrich). Media was replaced with half volume changes biweekly and cells were harvested seven days post-differentiation.

Lentiviral transduction and sgRNA cloning

A single guide RNA (sgRNA) to downregulate the expression of TDP-43 and a sgRNA control were selected from Horlbeck *et al.* (4), (5'-GGGAAGTCAGCCGTGAGACC-3' for *TARDBP* and 5'-GGACTAAGCGCAAGCACCTA-3' as control) and cloned into the SLQ1371-BFP-EF1A-puro lentiviral vector using the BstXI and BlpI restriction sites. HEK293T cells were used for packaging virus. Cells were seeded on tissue culture dishes coated with poly-D-lysine (Sigma-Aldrich) in Opti-MEM reduced serum media (Thermo Fisher Scientific) supplemented with 10% (v/v) FBS. The following day, the cells were transfected with individual sgRNA plasmids and the packaging vectors (psPAX2, pMD2.G and pAdVantage) in Opti-MEM using Lipofectamine 2000 (Invitrogen) as per the manufacturer's instructions. The next day, the media was replaced and two days later the media was filtered through a 0.45 µm syringe. Viral supernatant was used to transduce CRISPRi-i^{3}N iPSCs expressing dCas9-BFP-KRAB with individual sgRNAs. The following day the media was changed with Essential 8 Medium and two days after that, the transduced cells were selected with Essential 8 Medium supplemented with 1 µg/mL puromycin (Sigma-Aldrich).

Generation of TARDBP mutant and control human iPSC lines and motor neuron differentiation

All iPSC lines were derived from skin biopsy fibroblasts, collected under local ethical approval from Oxford and Edinburgh Ethics Committees. iPSC lines were derived from skin

biopsy fibroblasts in the James Martin Stem Cell Facility, University of Oxford, and The University of Edinburgh, under standardized published protocols. Transduced fibroblasts were plated for generation of iPSC clones, and clones were picked, expanded and banked as described previously (5). Clones from University of Oxford (OXTDP-01 and OXTDP-03) were derived using Cytotune 2.0™ (polycistronic vector Klf4–Oct3/4–Sox2, cMyc and Klf4 separate viruses), according to the manufacturer's instructions (Life Technologies, Rockville, MD, http://www.lifetech.com). Clones from The University of Edinburgh were generated using standard episomal reprogramming method (6). All iPSC lines passed quality control for genome integrity and expression of pluripotency markers (7). Motor neuron differentiation was performed using a previously published protocol (7, 8) and cells were cultured for 30 days, followed by harvesting for analysis. RNA was extracted from control- and TDP-43-mutant-iPSC-derived motor neurons using the miRNeasy kit (QIAGEN) following the manufacturer's protocol. RNA quality was determined by RNA Integrity Number (RIN) using RNA ScreenTape and reagents (Agilent) on the 2200 Tapestation System (Agilent). RNA-seq was performed using polyA libraries and sequenced on the HiSeq4000 to provide 150 bp paired-end reads.

Immunocytochemistry of iPSC-derived motor neurons

iPSC-derived motor neurons were seeded on glass coverslips, collected at day 30 of differentiation and fixed in 4% paraformaldehyde-phosphate buffered saline (PBS) for 15 min. Cells were permeabilized and blocked (10% donkey serum, 0.2% Triton X-100, in PBS) for 1h at room temperature, followed by incubation with primary antibodies (diluted in 1% donkey serum, 0.1% Triton X-100, in PBS) overnight at 4°C. The following primary antibodies were used: rabbit anti-TDP-43 (10782-2-AP, ProteinTech, 1:1000) and goat anti-Choline Acetyltransferase (ab144P, Millipore, 1:100). Alexa Fluor 488 donkey anti-rabbit and Alexa Fluor 647 donkey anti-goat (A32790 and A32849 respectively, ThermoFisher Scientific, 1:1000) diluted in 1% donkey serum and 0.1% Triton X-100 in PBS, were used to detect the corresponding antigen by incubating the cells for 1h at room temperature. Nuclei were stained with 4',6-Diamidino-2-Phenylindole (DAPI) in PBS for 5 min. Three PBS washes occurred between each incubation step. Finally, coverslips were mounted on microscope slides using fluorescence mounting medium (Dako) and fluorescent images were obtained using a confocal microscope Zeiss LSM 710 with the 63X objective.

To determine the cytoplasmic and nuclear TDP-43 content, 20-30 choline acetyltransferase (ChAT) positive cells for each clonal line and differentiation were analyzed using ImageJ software. Cytoplasm/nucleus (C/N) ratios were calculated using the mean intensity values for TDP-43 inside the ChAT-positive area (C) and in inside the DAPI-positive area (N). The average values of the C/N ratios per cell for each clonal line and differentiation were plotted.

Immunoblotting of iPSC-derived motor neurons

iPSC-derived motor neurons were harvested at day 30 of differentiation and lysed in RIPA buffer (ThermoFisher Scientific) supplemented with cOmpleteTM protease inhibitor cocktail (Sigma), homogenized with a pellet pestle and incubated on ice for 30 min. After centrifugation at 10,000 x g for 15 min the supernatant was collected and total protein concentration was determined using the PierceTM bicinchoninic acid assay (Sigma). A total of 10 µg of protein per sample were loaded and resolved on pre-cast NuPAGETM Bis-Tris 4-12% gradient gels (ThermoFisher Scientific) at 120V for 2.5 hours in MOPS running buffer

(Invitrogen). Samples were then transferred to nitrocellulose membranes at 20-25 V for 7 min using an iBlot 2 Dry blotting system (ThermoFisher Scientific). Blots were blocked for 1h at room temperature in Tris-buffered saline (TBS) supplemented with 0.1% Tween 20 and 5% skimmed milk. Incubation with primary antibodies (0.1% Tween 20, 1% milk, in TBS) were performed at 4°C overnight. The primary antibodies used were rabbit anti-TDP-43 (10782-2-AP, ProteinTech, 1:1000) and mouse anti-β actin (A5441, Sigma, 1:5,000). Horseradish peroxidase-conjugated anti-rabbit IgG or anti-mouse IgG (NA934 and NA931 respectively, Sigma) were used as secondary antibodies, and the signal was visualized in GE Healthcare Amersham Hyperfilm ECL using the ECL Plus detection system (both ThermoFisher Scientific). Three PBS washes occurred between each incubation step. The integrated optical density of each band was measured in ImageJ and expression was normalized to β-actin levels in the same blot for comparative expression assessment.

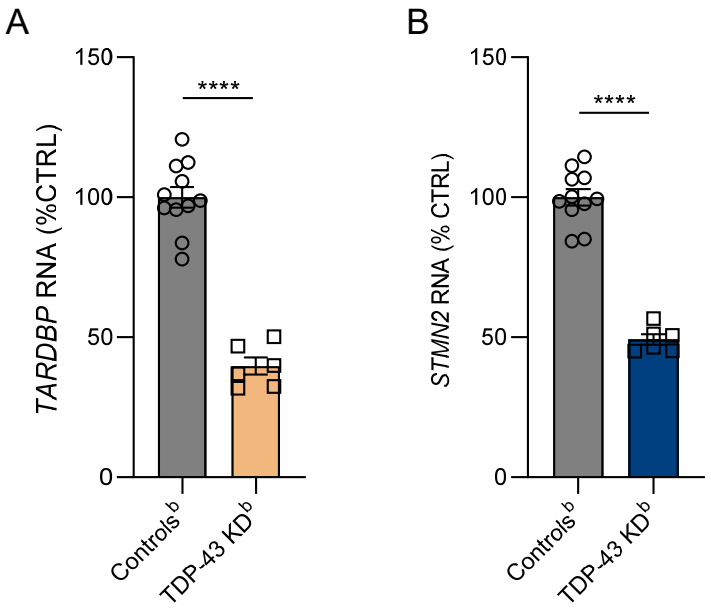

Supplementary Figure 1. *TARDBP* and *STMN2* RNA are reduced in iPSC-derived motor neuron data from Klim *et al*. in response to TDP-43 downregulation. Publicly available RNA-seq data from iPSC-derived motor neurons from Klim *et al*. was used to calculate RNA abundance as reads per kilobase per million (RPKM) and shown as a percent of controls. (**A**) *TARDBP* RNA is significantly reduced in the TDP-43 knockdown (TDP-43 KD) condition. (**B**) *STMN2* RNA levels were also significantly reduced in the TDP-43 KD condition, and as shown previously by Klim *et al*. Statistical differences were assessed by unpaired Student *t* tests: ****P<0.001. N=6 TDP-43 KD, N=11 Controls. Note truncated *STMN2* was upregulated in response to TDP-43 knockdown (see **Figure 1E**, dataset labeled "b")

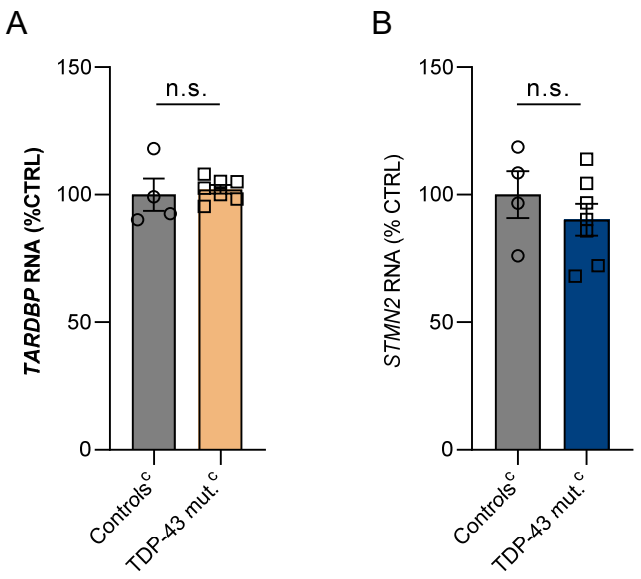

Supplementary Figure 2. *TARDBP* and *STMN2* RNA are not reduced in iPSC-derived motor neurons data with pathogenic *TARDBP* mutations. *TARDBP* (**A**) and *STMN2* (**B**) RNA levels in iPSC-derived motor neurons from patients with *TARDBP* mutations (TDP-43 mut.) or healthy controls (Controls) from a group in Edinburgh (dataset labeled "c" here and in **Figure 1E**), calculated as RPKM and shown as a percentage of control. Data show that mutations in TDP-43 alone do not lead to changes in either *TARDBP* or *STMN2* RNA levels. Statistical differences were assessed by unpaired Student *t* tests. n.s.: not significant differences. N=7 TDP-43 KD, N=4 Controls.

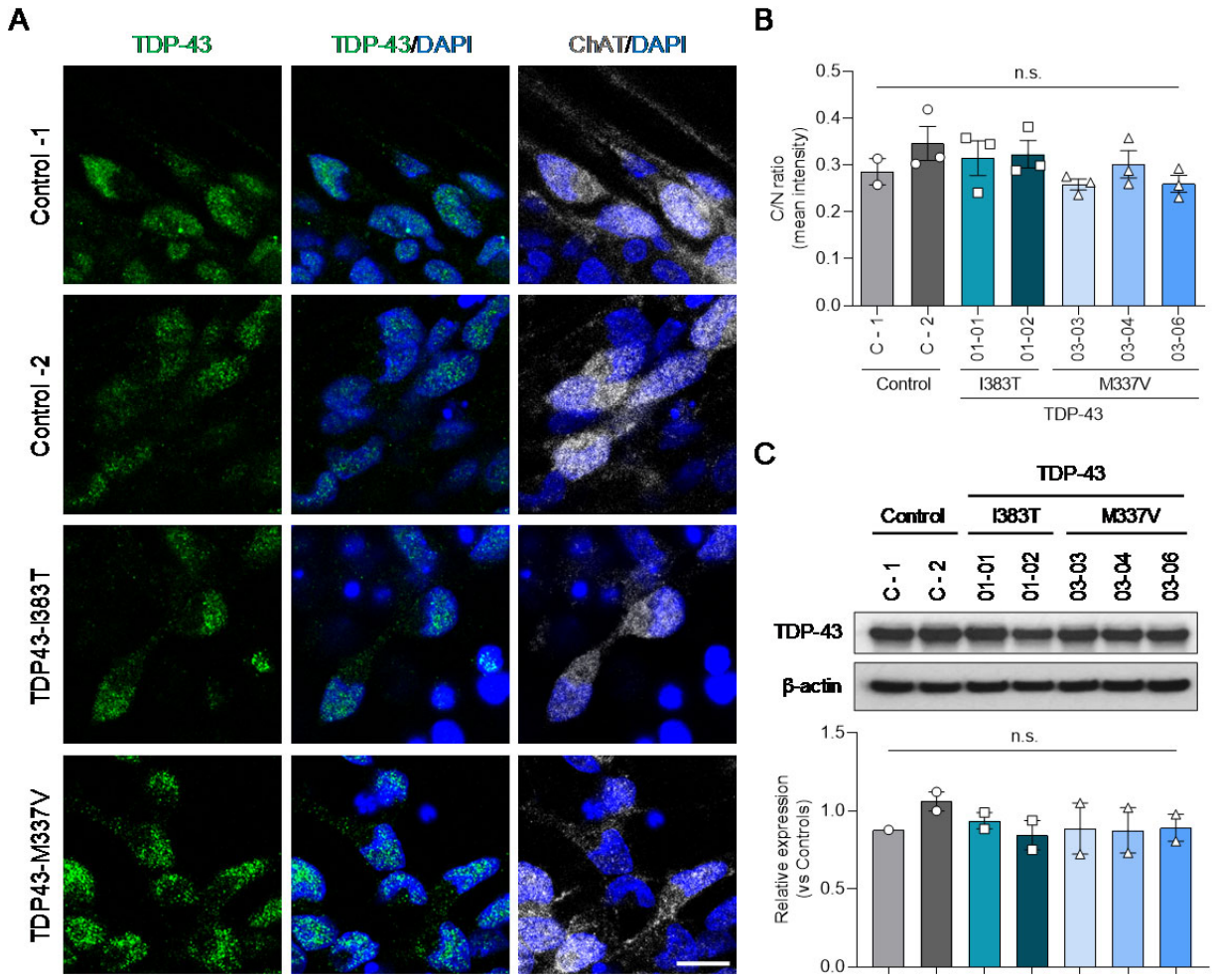

Supplementary Figure 3. TDP-43 levels and cellular location is not altered in iPSC-derived motor neurons with pathogenic *TARDBP* mutations. iPSC-derived motor neurons from patients with *TARDBP* mutations controls from a group in Oxford (dataset labeled "d" in **Figure 1E**) show no TDP-43 mislocalization, aggregation or change in TDP-43 protein levels. (**A**) TDP43-M337V and TDP43-I383T iPSC-derived motor neurons show similar nuclear-cytoplasmic distribution of TDP-43 (green) at day 30 of differentiation (DAPI in blue, Choline acetyltransferase (ChAT) in white). Scale bar indicates 10 µm. (**B**) Mean intensity of TDP-43 staining in the cytoplasm (stained with anti-ChAT) and inside the nucleus (DAPI) was analysed using ImageJ software to calculate the cytoplasm/nucleus (C/N) ratio for control (C – 1 and C – 2) and mutant (01-01, 01-02, 03-03, 03-04, 03-06) clones. N=3 independent differentiations (except in C - 1 where one of the differentiations failed) with SEM were plotted in the graph and no significant differences were observed. (**C**) The total quantity of soluble TDP-43 protein is not significantly different between the controls (C – 1 and C – 2) and the lines carrying TDP-43 mutations (01-01, 01-02, 03-03, 03-04, 03-06) at day 30 of differentiation. Unedited full gels are included as a **Supplementary File**. Relative TDP-43 expression values (standardized by β-actin levels) of 2 independent differentiations (except in C - 1 where one of the differentiations failed) were plotted in the graph. Statistical differences were assessed by one-way ANOVA. n.s.: not significant differences.

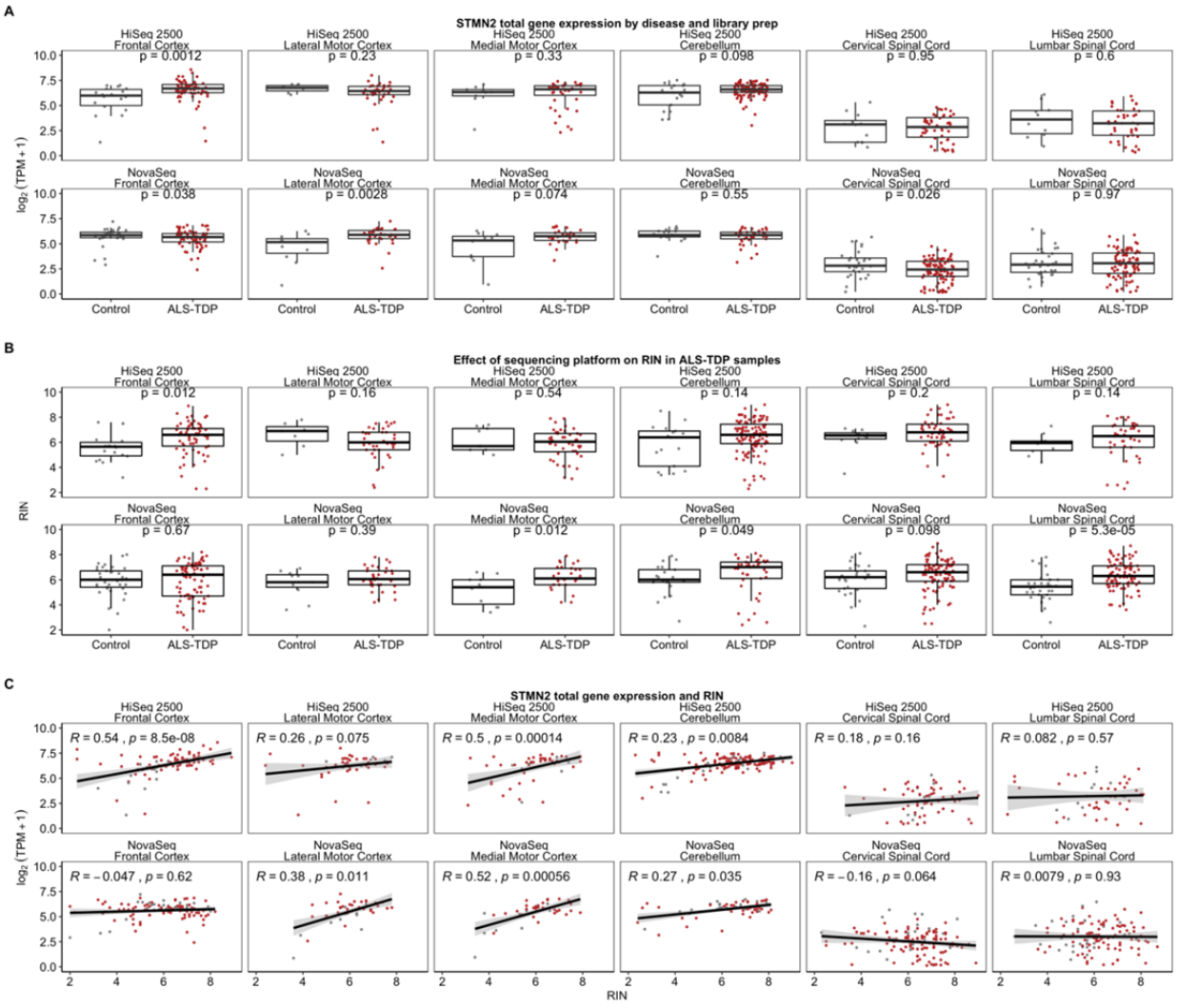

Supplementary Figure 4. The expression of full-length *STMN2* is influenced by technical factors. (**A**) Normalized transcripts per million of the full-length *STMN2* isoform in ALS-TDP (burgundy) versus control samples (grey) in the six tissues with the largest number of samples, and split by sequencing platform. (**B**) RNA integrity number (RIN), a measure of RNA quality, in ALS-TDP (burgundy) and control (grey) samples from all six tissues with the largest number of samples. (**A-B**) Data presented as box and whisker plots. These represent the median bounded by the first and third quartiles, with whiskers extending to 1.5 times the inter-quartile range. *P* values were calculated from Wilcoxon non-parametric test. (**C**) Correlations between RIN and full-length *STMN2* expression between tissue and sequencing platform in ALS-TDP. *P* values shown were calculated from Spearman correlations.

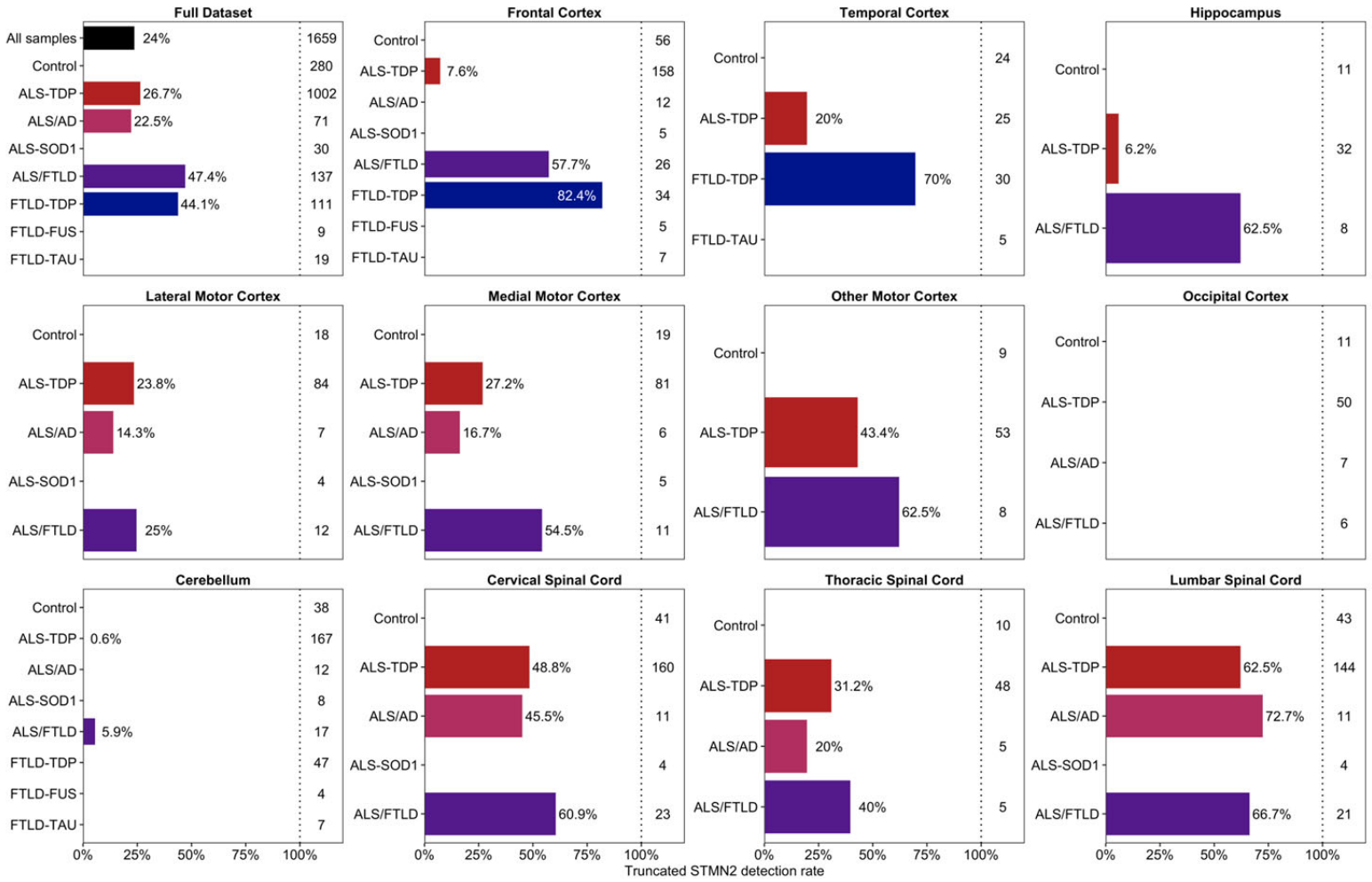

Supplementary Figure 5. Detection of the truncated *STMN2* isoform across the NYGC ALS Consortium dataset. Samples grouped by disease with or without TDP-43 pathology. Top left panel presents the entire dataset. Each group and tissue combination is presented as a proportion of that group where the truncated *STMN2* isoform could be detected. Bar graphs representing the proportion of individuals (%) with at least two reads spanning exon 1-exon 2a junction. The number of individuals with samples in indicated tissues/diseases is indicated on the right of the graph, after the vertical dotted line.

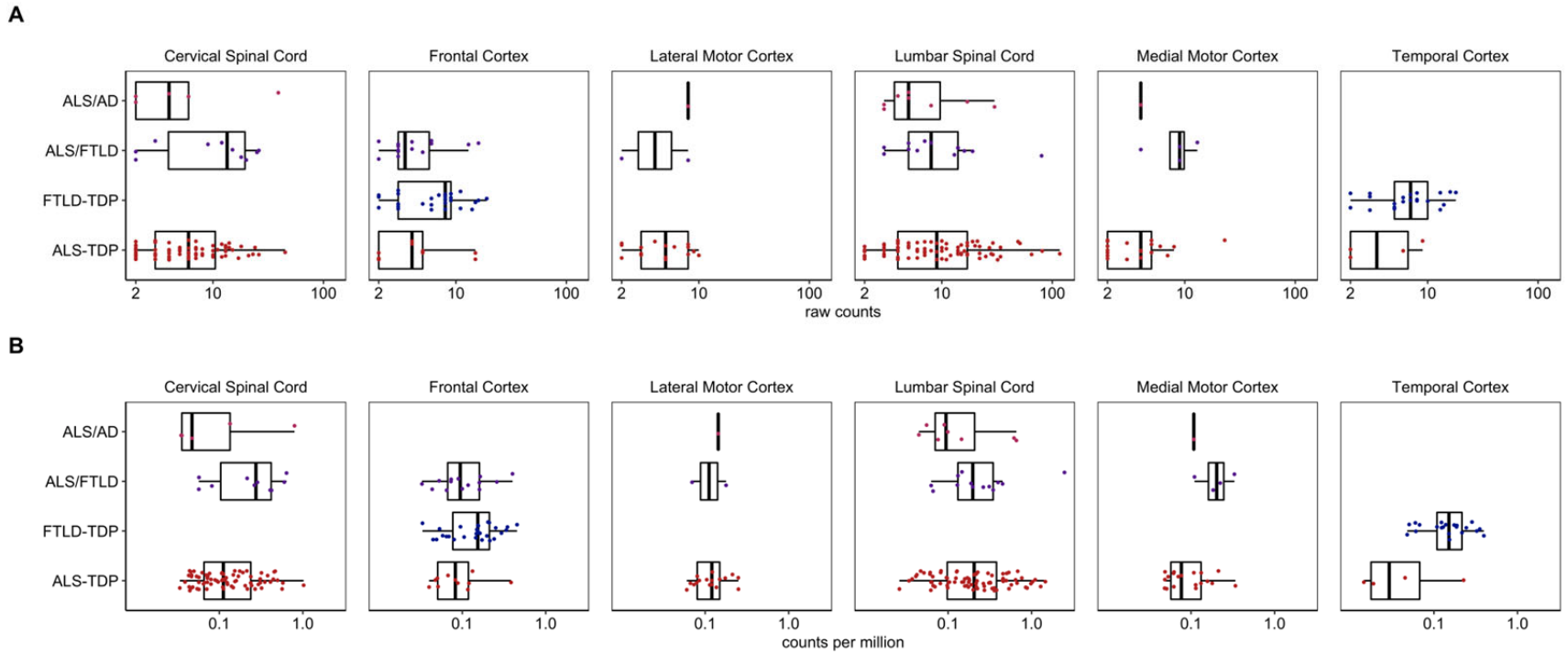

Supplementary Figure 6. Truncated *STMN2* expression across tissues and disease subtypes. Only samples with at least two reads and the six tissues with the most truncated *STMN2* RNA expression are shown. (**A**) Raw read counts for the truncated *STMN2* splice junction. X-axis is in log10 for illustrative purposes. (**B**) Normalized read counts per million for the truncated *STMN2* splice junction. Data is presented as box and whisker plots. These represent the median bounded by the first and third quartiles, with whiskers extending to 1.5 times the inter-quartile range.

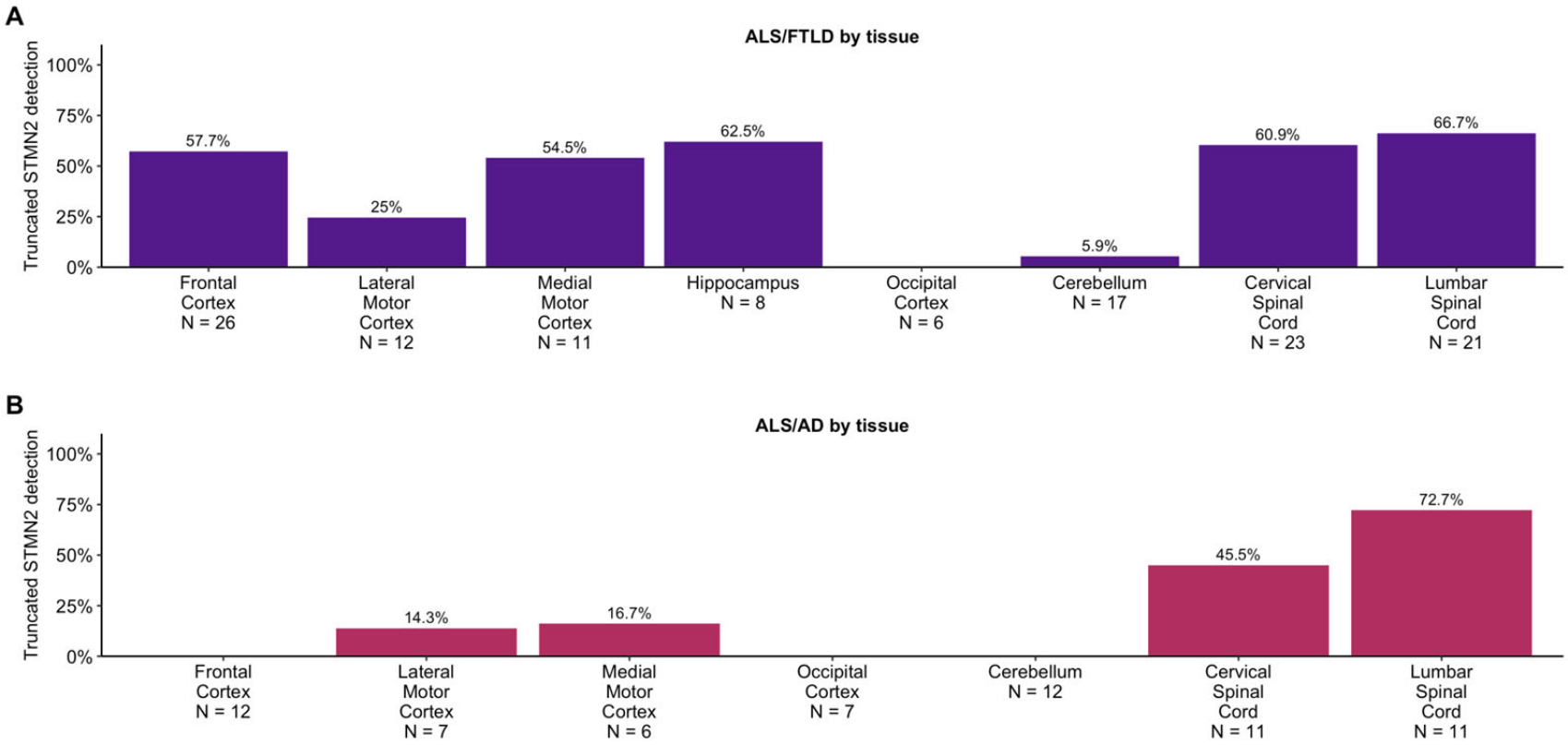

Supplementary Figure 7. Truncated *STMN2* detection rates for each major disease category across tissues. (**A**) In patients with concurrent ALS and FTD (ALS/FLTD) truncated *STMN2* RNA was detected in both cortical regions as well as in spinal cord, whereas (**B**) ALS patients with suspected Alzheimer's disease (ALS/AD) truncated *STMN2* RNA was most abundant in spinal cord but absent from the frontal cortex and relatively reduced levels were detected in motor cortical regions. Bar graphs representing the proportion of individuals (%) with at least two reads spanning exon 1-exon 2a junction. N refers to the number of individuals with samples in indicated tissues/diseases.

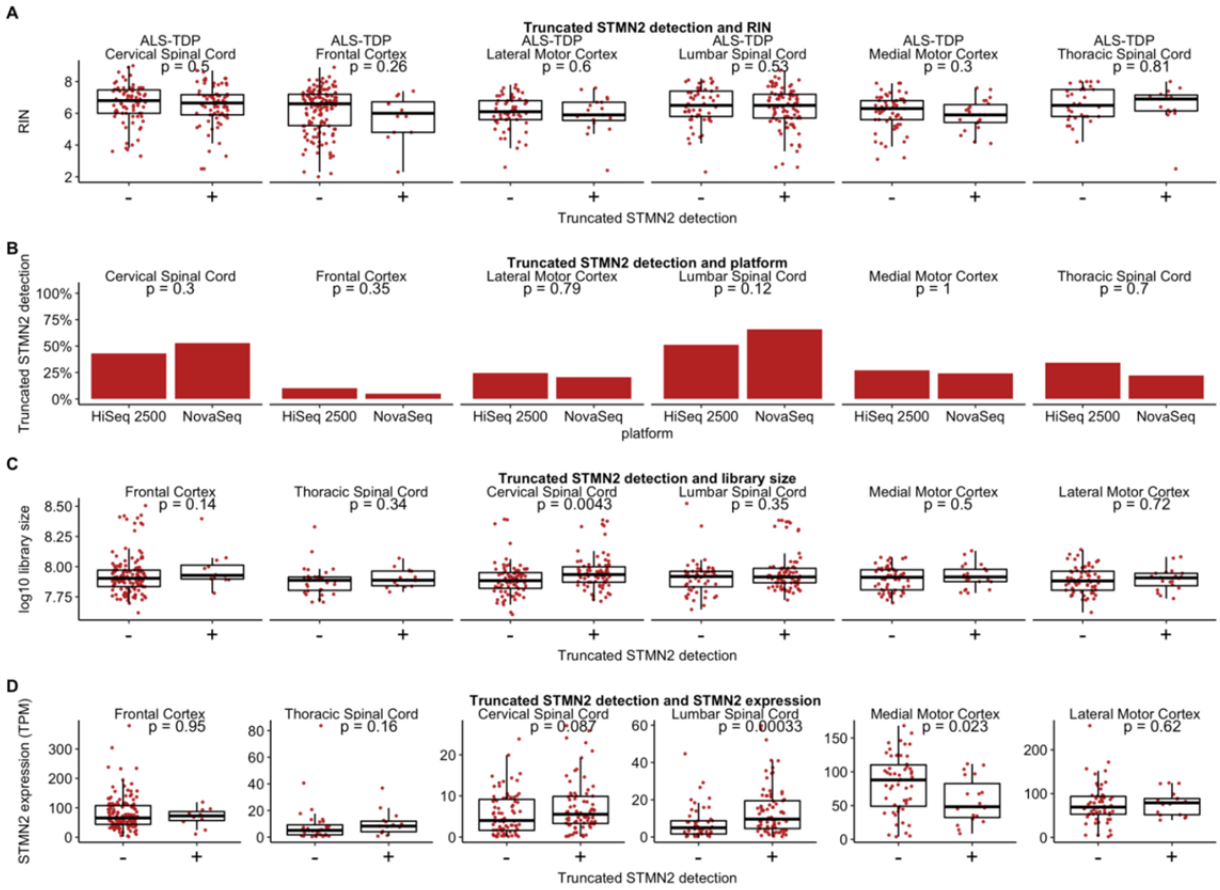

Supplementary Figure 8. Detection of truncated *STMN2* RNA is not influenced by technical factors. All samples presented are from the six tissues with the largest number of detectable truncated *STMN2* samples in ALS-TDP cases. (**A**) The distribution of RIN values between samples with detectable truncated *STMN2* (+) does not differ from samples without (-). (**B, C**) Detection rates are not influenced by RNA sequencing platform (**B**), nor dependent on total RNA-seq library size (log10 scale) (**C**). (**D**) Full-length *STMN2* expression levels differ in samples with and without detectable truncated *STMN2* RNA preliminarily in the lumbar spinal cord. Data in A, C, and D is presented as box and whisker plots. These present the median bounded by the first and third quartiles, with whiskers extending to 1.5 times the inter-quartile range. *P* values in A, C and D derive from a Wilcoxon non-parametric test. *P* values in B derive from a chi-squared test.

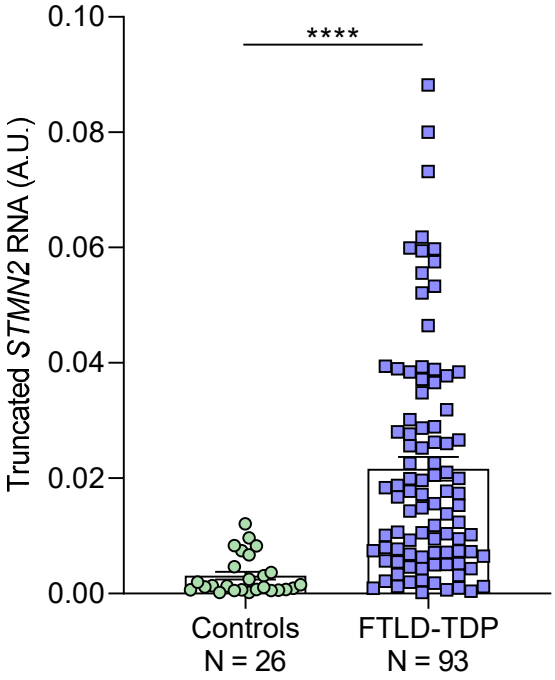

Supplementary Figure 9. Truncated *STMN2* is elevated in FTLD-TDP frontal cortex compared to controls, as measured by qRT-PCR. RNA was extracted from the frontal cortex of FTLD-TDP cases (N=93) and cognitive normal controls (N=26) to evaluate levels of truncated *STMN2* RNA by qRT-PCR. A total of 500 ng was used for qRT-PCR following same methods as described for the iPSC-derived neurons. Data is presented as mean ± SEM, and an unpaired Student *t* test was used to establish significant differences, ****P<0.0001.

Supplementary Table 1. Human iPSC lines used for *TARDBP* mutant and control motor neuron differentiations from Edinburgh and Oxford datasets.

Study	Patient group	Genotype	Sex	Age	Clone number	Differentiation number
Oxford	Control	Control	Female	60	1	1
						2
			Female	67	1	1
						2
Edinburgh			Male	64	1*	1
						2
			Female	56	1	1
						2
Oxford	ALS	*TARDBP* I383T	Male	60	1	1
						2
					2	1
						2
		TARDBP M337V	Male	57	1	1
						2
					2	1
						2
					3	1
						2
Edinburgh		*TARDBP* M337V	Male	59	1	1
						2
		TARDBP G288S	Male	64	1*	1
						2
						3
					2	1
						2

*Isogenic lines

Supplementary Table 2. Comparisons of truncated *STMN2* RNA in frontal cortex between FTLD-TDP cases and control cases.

			Unadjusted analysis		Adjusting for age at death, sex, and RIN		
Group	**N**	**Median (minimum, maximum) levels of truncated *STMN2* RNA**	**Regression coefficient (95% CI)**	**P-value**	**Regression coefficient (95% CI)**	**P-value**	**AUC (95% CI) vs. controls**
Controls	33	368 (26, 1336)	0.00 (reference)	NA	0.00 (reference)	NA	NA
All FTLD-TDP	238	560 (8, 5210)	0.86 (0.41, 1.32)	<0.001	0.60 (0.15, 1.06)	0.009	0.67 (0.57, 0.78)
FTLD-TDP type A	117	595 (8, 3495)	0.95 (0.43, 1.47)	<0.001	0.69 (0.17, 1.21)	0.010	0.70 (0.59, 0.80)
FTLD-TDP type B	66	494 (62, 5210)	0.76 (0.23, 1.29)	0.006	0.41 (-0.20, 1.01)	0.19	0.65 (0.53, 0.77)
FTLD-TDP type C	43	575 (106, 2071)	0.82 (0.26, 1.39)	0.005	0.46 (-0.12, 1.05)	0.12	0.67 (0.54, 0.80)
FTLD-TDP type D	2	1035 (1008, 1062)	1.88 (-0.21, 3.97)	0.076	1.44 (-0.67, 3.56)	0.17	0.94 (0.86, 1.02)

CI=confidence interval; AUC=area under the ROC curve. Regression coefficients, 95% CIs, and P-values result from linear regression models where the levels of truncated *STMN2* RNA in the frontal cortex were considered on the base 2 logarithm scale. Regression coefficients are interpreted as the difference in mean levels of truncated *STMN2* RNA in the frontal cortex (on the base 2 logarithm scale) between the given group of diseased patients and controls. P-values ≤ 0.010 are considered as statistically significant after applying a Bonferroni correction for multiple testing. NA: not applicable.

Supplementary Table 3. Comparisons of full-length *STMN2* RNA in frontal cortex between FTLD-TDP cases and control cases.

			Unadjusted analysis		Adjusting for age at death, sex, and RIN		
Group	**N**	**Median (minimum, maximum) levels of *STMN2***	**Regression coefficient (95% CI)**	**P-value**	**Regression coefficient (95% CI)**	**P-value**	**AUC (95% CI) vs. controls or PSP cases**
Controls	33	17558 (2338, 61245)	0.00 (reference)	NA	0.00 (reference)	NA	NA
PSP	41	9258 (1866, 31170)	-0.69 (-0.98, -0.40)	<0.001	-0.81 (-1.13, -0.48)	<0.001	0.83 (0.73, 0.93)
Controls	33	17558 (2338, 61245)	0.00 (reference)	NA	0.00 (reference)	N/A	NA
FTLD-TDP	238	11832 (1418, 96495)	-0.50 (-0.74, -0.25)	<0.001	-0.60 (-0.84, -0.35)	<0.001	0.74 (0.65, 0.84)
PSP	41	9258 (1866, 31170)	0.00 (reference)	NA	0.00 (reference)	NA	NA
FTLD-TDP	238	11832 (1418, 96495)	0.19 (-0.03, 0.41)	0.085	0.15 (-0.06, 0.37)	0.15	0.60 (0.51, 0.68)

CI=confidence interval; AUC=area under the ROC curve. Regression coefficients, 95% CIs, and P-values result from linear regression models where the levels of full-length *STMN2* RNA in the frontal cortex were considered on the base 2 logarithm scale. Regression coefficients are interpreted as the difference in mean levels of full-length *STMN2* RNA in the frontal cortex (on the base 2 logarithm scale) between the given group of diseased patients and the reference group (controls or PSP cases). P-values <0.0167 are considered as statistically significant after applying a Bonferroni correction for multiple testing. NA: not applicable.

Supplementary Table 4. Associations of interest of full-length *STMN2* RNA in FTLD-TDP frontal cortex.

	Unadjusted analysis		Multivariable analysis		
Variable	**Regression coefficient (95% CI)**	**P-value**	**Regression coefficient (95% CI)**	**P-value**	**Multivariable model adjustments**
pTDP-43 (doubling)	0.05 (-0.02, 0.12)	0.15	0.02 (-0.05, 0.10)	0.53	Age at death, sex, TDP-43 subtype
TDP-43 subtype	Overall test of difference: P=0.037		Overall test of difference: P=0.012		Age at death and sex
FTLD-TDP type A	0.00 (reference)	NA	0.00 (reference)	NA	
FTLD-TDP type B	-0.37 (-0.66, -0.09)	0.011	-0.46 (-0.76, -0.15)	0.004	
FTLD-TDP type C	-0.22 (-0.54, 0.11)	0.19	-0.24 (-0.57, 0.08)	0.15	
FTLD-TDP type D	-1.10 (-2.33, 0.12)	0.078	-1.23 (-2.47, 0.01)	0.052	
Age at onset (10 year increase)	-0.02 (-0.17, 0.13)	0.78	-0.13 (-0.29, 0.02)	0.095	Sex and TDP-43 subtype
Survival after onset (5 year increase)	-0.01 (-0.15, 0.13)	0.88	-0.05 (-0.20, 0.10)	0.49	Age at onset, sex, and TDP-43 subtype
Sex (male)	-0.14 (-0.39, 0.11)	0.28	-0.18 (-0.44, 0.07)	0.15	Age at death and TDP-43 subtype

CI=confidence interval. Regression coefficients, 95% CIs, and P-values result from linear regression models, where frontal cortex full-length *STMN2* RNA was considered on the base 2 logarithm scale. Regression coefficients are interpreted as the change in mean frontal cortex full-length *STMN2* RNA (on the base 2 logarithm scale) corresponding to presence of the given characteristic (categorical variables) or the increase given in parenthesis (continuous variables). P-values ≤ 0.010 are considered as statistically significant after applying a Bonferroni correction for multiple testing. NA: not applicable.

Supplementary Table 5. List of NanoString Plexset probes used to quantify *STMN2* splicing in post-mortem brain.

Identifier	Accession	Region	Target sequence
Truncated *STMN2*	-	10-109	AGAAGACCTTCGAGAGAAAGGTAGAAAATAAGAATTTGGCTCTCTGTGTGAGCATGTGTGCGTG TGTGCGAGAGAGAGAGACAGACAGCCTGC
Full-length *STMN2*	NM_007029.2	106-205	TCACTGATCTGCTCTTGCTTTTACCCGGAACCTCGCAACATCAACATCTATACTTACGATGATATG GAAGTGAAGCAAATCAACAAACGTGCCTCTGGCC
HPRT1	NM_000194.3	428-527	CTATGACTGTAGATTTTATCAGACTGAAGAGCTATTGTAATGACCAGTCAACAGGGGACATAAA AGTAATTGGTGGAGATGATCTCTCAACTTTAACTGG

Supplementary References

1. Wang C, Ward ME, Chen R, Liu K, Tracy TE, Chen X, Xie M, Sohn PD, Ludwig C, Meyer-Franke A, et al. Scalable Production of iPSC-Derived Human Neurons to Identify Tau-Lowering Compounds by High-Content Screening. *Stem Cell Reports.* 2017;9(4):1221-33.
2. Tian R, Gachechiladze MA, Ludwig CH, Laurie MT, Hong JY, Nathaniel D, Prabhu AV, Fernandopulle MS, Patel R, Abshari M, et al. CRISPR Interference-Based Platform for Multimodal Genetic Screens in Human iPSC-Derived Neurons. *Neuron.* 2019.
3. Fernandopulle MS, Prestil R, Grunseich C, Wang C, Gan L, and Ward ME. Transcription Factor-Mediated Differentiation of Human iPSCs into Neurons. *Curr Protoc Cell Biol.* 2018;79(1):e51.
4. Horlbeck MA, Gilbert LA, Villalta JE, Adamson B, Pak RA, Chen Y, Fields AP, Park CY, Corn JE, Kampmann M, et al. Compact and highly active next-generation libraries for CRISPR-mediated gene repression and activation. *Elife.* 2016;5(
5. Dafinca R, Scaber J, Ababneh N, Lalic T, Weir G, Christian H, Vowles J, Douglas AG, Fletcher-Jones A, Browne C, et al. C9orf72 Hexanucleotide Expansions Are Associated with Altered Endoplasmic Reticulum Calcium Homeostasis and Stress Granule Formation in Induced Pluripotent Stem Cell-Derived Neurons from Patients with Amyotrophic Lateral Sclerosis and Frontotemporal Dementia. *Stem Cells.* 2016;34(8):2063-78.
6. Johnstone M, Vasistha NA, Barbu MC, Dando O, Burr K, Christopher E, Glen S, Robert C, Fetit R, Macleod KG, et al. Reversal of proliferation deficits caused by chromosome 16p13.11 microduplication through targeting NFkappaB signaling: an integrated study of patient-derived neuronal precursor cells, cerebral organoids and in vivo brain imaging. *Mol Psychiatry.* 2019;24(2):294-311.
7. Dafinca R, Barbagallo P, Farrimond L, Candalija A, Scaber J, Ababneh NA, Sathyaprakash C, Vowles J, Cowley SA, and Talbot K. Impairment of Mitochondrial Calcium Buffering Links Mutations in C9ORF72 and TARDBP in iPS-Derived Motor Neurons from Patients with ALS/FTD. *Stem Cell Reports.* 2020;14(5):892-908.
8. Selvaraj BT, Livesey MR, Zhao C, Gregory JM, James OT, Cleary EM, Chouhan AK, Gane AB, Perkins EM, Dando O, et al. C9ORF72 repeat expansion causes vulnerability of motor neurons to Ca(2+)-permeable AMPA receptor-mediated excitotoxicity. *Nat Commun.* 2018;9(1):347.

SUPPLEMENTARY ACKNOWLEDGMENTS

NYGC ALS Consortium members and sites.

#	Site	PI Name
1	Center for Genomics of Neurodegenerative Disease (CGND), New York Genome Center, New York, NY	Hemali Phatnani, PhD
2	Department of Neurology, Lewis Katz School of Medicine, Temple University, Philadelphia, PA	Justin Kwan, MD
3	Cedars-Sinai Department of Biomedical Sciences, Board of Governors Regenerative Medicine Institute and Brain Program, Cedars-Sinai Medical Center, and Department of Medicine, University of California, Los Angeles, CA	Dhruv Sareen, PhD
4	Department of Biochemistry and Molecular Biology, Penn State Institute for Personalized Medicine, The Pennsylvania State University, Hershey, PA	James R. Broach, PhD
5	Department of Neurology, The Pennsylvania State University, Hershey, PA	Zachary Simmons, MD
6	Department of Neurology, Henry Ford Health System, Detroit, MI	Ximena Arcila-Londono, MD
7	Department of Pathology and Laboratory Medicine, Perelman School of Medicine, University of Pennsylvania, Philadelphia, PA	Edward B. Lee, MD, PhD
8	Department of Pathology and Laboratory Medicine, Perelman School of Medicine, University of Pennsylvania, Philadelphia, PA	Vivianna M. Van Deerlin, MD, PhD
9	Department of Neurology, Center for Motor Neuron Biology and Disease, Institute for Genomic Medicine, Columbia University, New York, NY	Neil A. Shneider, MD, PhD
10	Department of Biological Engineering, Massachusetts Institute of Technology, Cambridge, MA	Ernest Fraenkel, PhD
11	Department of Neurology, Johns Hopkins School of Medicine, Baltimore, MD	Lyle W. Ostrow, MD, PhD
12	Department of Neurogenetics, Academic Medical Centre, Amsterdam and Leiden University Medical Center, Leiden, The Netherlands	Frank Baas, MD, PhD
13	Department of Medicine, Lung Biology Center, University of California, San Francisco, CA	Noah Zaitlen, PhD
14	ALS Multidisciplinary Clinic, Neuromuscular Division, Department of Neurology, Harvard Medical School, and Neurological Clinical Research Institute, Massachusetts General Hospital, Boston, MA	James D. Berry, MD, MPH
15	Centre for Neuroscience and Trauma, Blizard Institute, Barts and The London School of Medicine and Dentistry, Queen Mary University of London, London, and Department of Neurology, Basildon University Hospital, Basildon, United Kingdom	Andrea Malaspina, MD, PhD
16	Institute of Neurology, National Hospital for Neurology and Neurosurgery, University College London, London, United Kingdom	Pietro Fratta, MD, PhD
17	The Jackson Laboratory, Bar Harbor, ME	Gregory A. Cox, PhD
18	Department of Psychiatry & Human Behavior, Department of Biological Chemistry, School of Medicine, and Department of Neurobiology and Behavior, School of Biological Sciences, University California, Irvine, CA	Leslie M. Thompson, PhD
19	Taube/Koret Center for Neurodegenerative Disease Research, Roddenberry Center for Stem Cell Biology and Medicine, Gladstone Institute	Steve Finkbeiner, MD, PhD

20	Department of Neurology & Sensory Organs, University of Thessaly, Thessaly, Greece	Efthimios Dardiotis, MD, PhD
21	Department of Neurology ,Washington University in St. Louis, St. Louis, MO	Timothy M. Miller, MD, PhD
22	Centre for Clinical Brain Sciences, Anne Rowling Regenerative Neurology Clinic, Euan MacDonald Centre for Motor Neurone Disease Research, University of Edinburgh, Edinburgh, United Kingdom	Siddharthan Chandran, PhD
23	Centre for Clinical Brain Sciences, Anne Rowling Regenerative Neurology Clinic, Euan MacDonald Centre for Motor Neurone Disease Research, University of Edinburgh, Edinburgh, United Kingdom	Suvankar Pal, MD
24	Department of Molecular Genetics, Weizmann Institute of Science, Rehovot, Israel	Eran Hornstein, MD, PhD
25	Department of Neurology, Icahn School of Medicine at Mount Sinai, New York, NY	Daniel J. MacGowan, MD
26	Center for Neurodegenerative Disorders, Department of Neurology, the Lewis Katz School of Medicine, Temple University, Philadelphia, PA	Terry Heiman-Patterson, MD
27	Cold Spring Harbor Laboratory, Cold Spring Harbor, NY	Molly G. Hammell, PhD
28	Computer Science and Systems Biology Program, Ann Romney Center for Neurological Diseases, Department of Neurology and Division of Genetics in Department of Medicine, Brigham and Women's Hospital, Boston, MA, Harvard Medical School, Boston, MA, and Program in Medical and Population Genetics, Broad Institute, Cambridge, MA	Nikolaos. A. Patsopoulos, MD, PhD
29	Ann Romney Center for Neurologic Diseases, Brigham and Women's Hospital, Harvard Medical School, Boston, MA	Oleg Butovsky, PhD
30	Department of Anesthesiology, Stony Brook University, Stony Brook, NY	Joshua Dubnau, PhD
31	Section of Infections of the Nervous System, National Institute of Neurological Disorders and Stroke, NIH, Bethesda, MD	Avindra Nath, MD
32	Department of Neurology, Barrow Neurological Institute, St. Joseph's Hospital and Medical Center, Department of Neurobiology, Barrow Neurological Institute, St. Joseph's Hospital and Medical Center, Phoenix, AZ	Robert Bowser, PhD
33	Department of Neurology, Division of Neuromuscular Medicine, Columbia University, New York, NY	Matt Harms, MD
34	Department of Neuropathology, Academic Medical Center, University of Amsterdam, Amsterdam, The Netherlands	Eleonora Aronica, MD, PhD
35	Department of Biology and Veterinary and Biomedical Sciences, The Pennsylvania State University, University Park, PA	Mary Poss, DVM, PhD
36	New York Stem Cell Foundation, Department of Bioengineering, School of Engineering and Applied Sciences, University of Pennsylvania, Philadelphia, PA	Jennifer Phillips-Cremins, PhD
37	Department of Pathology, Fishberg Department of Neuroscience, Friedman Brain Institute, Ronald M. Loeb Center for Alzheimer's Disease, Icahn School of Medicine at Mount Sinai, New York, NY	John Crary, MD, PhD
38	Department of Neurology, Harvard Medical School, Neurological Clinical Research Institute, Massachusetts General Hospital, Boston, MA	Nazem Atassi, MD
39	Department of Neurology, Hospital for Special Surgery and Weill Cornell Medical Center, New York, NY	Dale J. Lange, MD
40	Medical Genetics, Atlantic Health System, Morristown Medical Center, Morristown, NJ, and Overlook Medical Center, Summit, NJ	Darius J. Adams, MD
41	Center of Clinical Research, Experimental Surgery and Translational Research, Biomedical Research Foundation	Leonidas Stefanis, MD, PhD

	of the Academy of Athens (BRFAA), 4 Soranou Efesiou Street, 11527, Athens, Greece; 1st Department of Neurology, Eginition Hospital, Medical School, National and Kapodistrian University of Athens, Athens, Greece	
42	Neuromuscular/EMG service and ALS/Motor Neuron Disease Clinic , Hebrew University-Hadassah Medical Center, Jerusalem, Israel	Marc Gotkine, MD
43	Board of Governors Regenerative Medicine Institute, Los Angeles, CA; Department of Neurology, Cedars-Sinai Medical Center, Los Angeles, CA	Robert H. Baloh, MD. PhD
44	Neurological Clinical Research Institute, Massachusetts General Hospital, Boston, MA	Suma Babu, MBBS, MPH
45	Departments of Neuroscience, and Genetics and Genomic Sciences, Ronald M. Loeb Center for Alzheimer's disease, Icahn School of Medicine at Mount Sinai, New York, NY	Towfique Raj, PhD
46	Harvard Medical School, Department of Physical Medicine & Rehabilitation, Spaulding Rehabilitation Hospital, Boston, MA	Sabrina Paganoni, MD, PhD
47	Center for Cellular and Molecular Therapeutics, Children's Hospital of Philadelphia, Philadelphia, PA; Department of Genetics, Perelman School of Medicine, University of Pennsylvania, Philadelphia, PA	Ophir Shalem, PhD
48	Centre for Clinical Brain Sciences, University of Edinburgh, Edinburgh, UK; Euan MacDonald Centre for Motor Neurone Disease Research, University of Edinburgh, Edinburgh, UK	Colin Smith, MD
49	Department of Genetics and Genomic Sciences, Icahn Institute of Data Science and Genomic Technology, Icahn School of Medicine at Mount Sinai, New York, NY	Bin Zhang, PhD
50	University of Maryland Brain and Tissue Bank and NIH NeuroBioBank	
51	Department of Neuropathology, Georgetown Brain Bank, Georgetown Lombardi Comprehensive Cancer Center, Georgetown University Medical Center, Washington DC	Brent Harris, MD, PhD
52	Neuroradiology Section, Department of Radiology and Biomedical Imaging, University of California, San Francisco, San Francisco, CA	Iris Broce, PhD
53	Neuromuscular Diseases Unit, Department of Neurology, Tel Aviv Sourasky Medical Center, Sackler Faculty of Medicine, Tel-Aviv University, Tel-Aviv, Israel	Vivian Drory, MD
54	Department of Neuroscience, University of California San Diego, La Jolla, CA	John Ravits, MD
55	Department of Neurology, University of Pennsylvania Perelman School of Medicine, Philadelphia, PA	Corey McMillan, PhD
56	Department of Neurology, Columbia University Medical Center, New York, NY	Vilas Menon, PhD

Full unedited gels for Supplementary Figure 3C

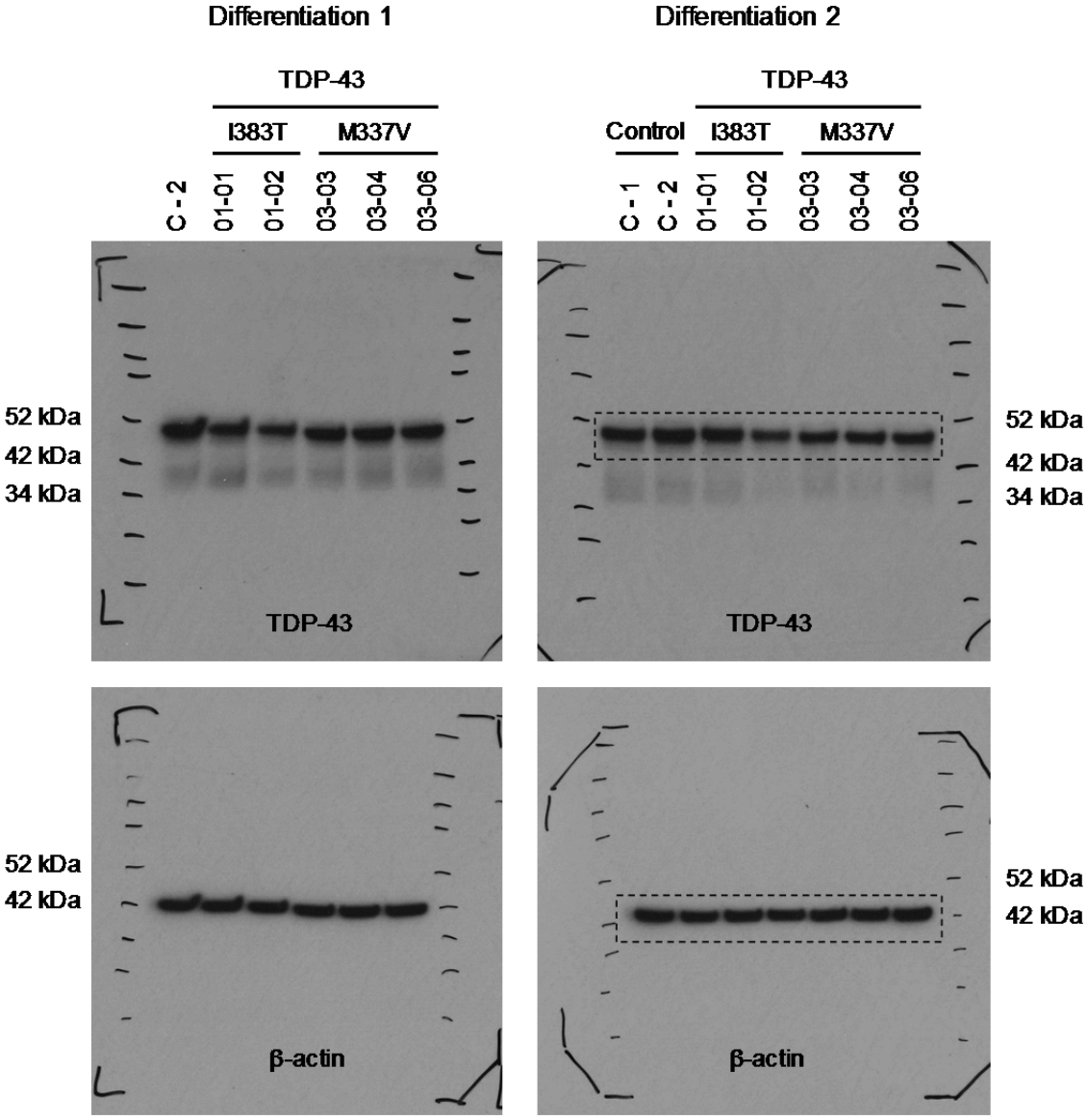

Full unedited gels for Supplementary Figure 3C. Unedited gels for TDP-43 and β-actin are included here for all the samples represented in the relative quantification graph in **Supplementary Figure 3C**. The portion of the gel images shown in **Supplementary Figure 3C** are denoted with the dashed squares.